BRNO UNIVERSITY OF TECHNOLOGY
VYSOKÉ UČENÍ TECHNICKÉ V BRNĚ

FACULTY OF MECHANICAL ENGINEERING
FAKULTA STROJNÍHO INŽENÝRSTVÍ

INSTITUTE OF AEROSPACE ENGINEERING
LETECKÝ ÚSTAV

LOAD STATE OF AN AIRCRAFT WITH AN ELASTIC WING
ZATÍŽENÍ LETOUNU PŘI VELKÝCH DEFORMACÍCH KŘÍDLA

DOCTORAL THESIS
DIZERTAČNÍ PRÁCE

AUTHOR — **Ing. Pavel Schoř**
AUTOR PRÁCE

SUPERVISOR — **prof. Ing. Antonín Píštěk, CSc.**
ŠKOLITEL

BRNO 2018

Abstrakt

V této práci je navržena metoda výpočtu zatížení letadla s netuhým křídlem, založená na spojení panelové metody prvního řádu dle Katz and Plotkin, Low-Speed Aerodynamics, 2001 s metodou stukturální analýzy dle Píštěk et al., Pevnost a životnost letadel I, 1988 a Lebofsky,Numerically Generated Tangent Stiffness Matrices for Geometrically Non-Linear Structures, 2013. Panelová metoda poskytuje přasná data pro výpočet zatížení křídla od vzdušných sil za předpokladu že lze dané proudění aproximovat pomocí potenciálního proudění, Narozdíl metod založených na interakci s CFD metodami lze navrženou metodu používat i na bežném počítači.

Summary

This thesis proposes a methodology, how to calculate the load state of an aircraft with an elastic wing by first-order panel panel method according to Katz and Plotkin, Low-Speed Aerodynamics, 2001 coupled to a structural analysis method according to Píštěk et al., Pevnost a životnost letadel I, 1988 and Lebofsky,Numerically Generated Tangent Stiffness Matrices for Geometrically Non-Linear Structures, 2013. For a flow, which is similar to a potential flow, panel methods can provide an accurate information about all characteristics required for a calculation of aerodynamic load. Unlike the CFD based methods, this method can be used on an average personal computer.

Klíčová slova

Letadlo, Letoun, Kluzák, Aerodynamika, Simulace letu, Výpočet zatížení, Elastické křídlo

Keywords

Aircraft, Aeroplane, Sailplane,Aerodynamics, Flight simulation, Load calculation, Elastic wing

SCHOŘ P.*Zatížení letounu při velkých deformacích křídla.* Brno: Vysoké učení technické v Brně, Fakulta strojního inženýrství, 2018. 35 s. Vedoucí dizertační práce prof. Ing. Antonín Píštěk, CSc..

I, PAVEL SCHOŘ, declare that this thesis titled, LOAD STATE OF AN AIRCRAFT WITH AN ELASTIC WING and the work presented in it are my own. I confirm that:

- This work was done mainly while in candidature for a research degree at Brno University of Technology.
- Where any part of this thesis has previously been submitted for a degree or any other qualification at this University or any other institution, this has been clearly stated.
- Where I have consulted the published work of others, this is always clearly attributed.
- Where I have quoted from the work of others, the source is always given. With the exception of such quotations, this thesis is entirely my own work.
- I have acknowledged all main sources of help.

Ing. Pavel Schoř

Contents

Chapter 1

Introduction

1.1 Scope of this thesis

A main goal of this thesis is to develop a methodology for computing aerodynamic loads of aircraft with highly elastic wings. A key assumption is that the deformation progresses slowly in time. Therefore only static aeroelastic phenomena are studied. The method should be affordable for any aircraft design organization in matters of simplicity and computational costs. Although the name of the thesis is "Load state of an aircraft with an elastic wing", only modern sailplanes are evaluated in this thesis. A main reason for this is that modern sailplanes are kind aircraft, which mostly exhibit large deformations of their wings. Next, it is very easy to extend the presented method for analysis of airplane by simply adding the propulsion force into equations of motion. Also any powered airplane becomes a sailplane, once the engine stops.With minor modifications [4], this method can be applied also to other kind of aircrafts, including rotorcrafts and flapping wings.

1.2 Static aeroelasticity

The aerodynamic forces acting on a surface of the sailplane's wing may change its shape significantly when the stiffness of the wing is low. For instance, when witnessing a strength test of a glider wing as shown on Figure 1.1, one may naturally ask how the aerodynamic forces have changed due the deformation. According to airworthiness regulations, it is necessary to take this air load redistribution into account. The EASA CS22 regulation explicitly states in paragraph CS22.301(C): "If deflections under load would significantly change the distribution of external or internal loads, this redistribution must be taken to account."[5]

Figure 1.1: A strength test of glider wing at IAE Brno University of Technology

1.2.1 Motivation

A very strong motivation for detailed study of the static aeroelasticity was the event of destruction of NASA Helios HP03-2 in June 26, 2003. According to the mishap report, the Helios encountered an atmospheric turbulence, as a result of this, the wingtip deflection increased to 12 meters, as shown on Figure 1.2. After this, the Helios experienced several pitch oscillations, the last one resulted in the failure of the leading edge structure, the main spar remained undamaged as shown on Figure 1.3. In the mishap report, the NASA has described the methodology how the Helios was designed and how the effect of the wing bending was simulated. First, the aerodynamic load of the undeformed wing was computed using VSAERO[4], then the deformed shape was computed using NASTRAN. Second, the aerodynamic load of the deformed wing was again computed using VSAERO. This load iterations were done manually. The NASA explicitly calls this approach as insufficient and sets a need for a new robust tool, which is able to compute the redistribution of the aerodynamic load on a flexible wing.

Figure 1.2: The Helios aircraft undergoing large deformation [6]

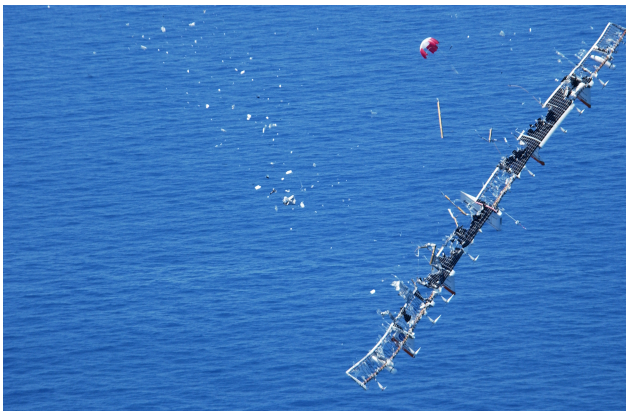

Figure 1.3: The Helios aircraft after structural failure during flight [6]

Chapter 2

Governing equations

2.1 Domain decomposition

In this thesis a problem of flight of an elastic aircraft is solved in three different domains. The forces acting on the surface of the aircraft are solved in Flow domain. The deformation of the aircraft is solved in Structural domain. When an equilibrium between the aerodynamic and internal forces in the structure is found, the resulting aerodynamic force is passed into Flight dynamics domain, where a flight condition for next time step is computed. If a quasi static solution is desired, then only interaction between flow and structural domain is used. In this chapter only governing equations for each domain are presented, solution and interaction procedures are presented in Chapter 4.

2.2 Flow domain

2.2.1 Navier-Stokes Equations

A motion of an incompressible fluid can be described by Equation (2.1) and Equation (2.2) [1]. The first equation represent a conservation of mass and the second equation represent a conservation of momentum. These equations must be satisfied for each infinitesimally small volume of the fluid. These small volumes are called particles. The Equation (2.1) and Equation (2.2) are called Navier-Stokes equations for incompressible fluid (with constant viscosity coefficient) [1].

$$\nabla \cdot \mathbf{u} = 0 \tag{2.1}$$

$$\rho\left(\frac{\partial \mathbf{u}}{\partial t} + \mathbf{u}\cdot\nabla\mathbf{u}\right) = \rho\mathbf{f} - \nabla p + \mu\nabla^2 u \tag{2.2}$$

In Equation (2.1) and Equation (2.2):
$\mathbf{u}$ is velocity vector
$\mathbf{f}$ is vector of body forces
ρ is fluid density
μ is kinematic viscosity

2.2.2 Laplace's Equation

Solving the Navier-Stokes equations provides an accurate model of the flow, but solution of these equations requires enormous effort. If the flow can be assumed as inviscid, incompressible and irrotational, then velocity potential Φ can be introduced and velocity at each point can be obtained as its gradient. This flow can be described by Equation (2.4) and the complexity of the problem is reduced significantly. This flow is traditionally called a potential flow.

The scalar function Φ is introduced in Equation (2.3). This function is called velocity potential and velocity $\overrightarrow{u}$ at each point can be obtained by its derivation:

$$\mathbf{u} = \nabla\Phi \tag{2.3}$$

Substituting Equation (2.3) into Equation (2.1) gives Laplace's Equation (2.4), which also represents a continuity equation for the potential flow.

$$\nabla\cdot\mathbf{u} = \nabla\cdot\nabla\Phi = \nabla^2\Phi = 0 \tag{2.4}$$

The momentum equation for the potential flow can be expressed as:

$$\nabla\left(E + \frac{p}{\rho} + \frac{u^2}{2} + \frac{\partial\Phi}{\partial t}\right) = 0 \tag{2.5}$$

In Equation (2.5), the E represents a potential of conservative body forces $\mathbf{f}$:

$$\mathbf{f} = -\nabla E \tag{2.6}$$

The main advantage of the potential flow is a very low demand for computational power. Various methods can be used to obtain the velocity potential, see Chapter 3, Section 3.1. Although the potential flow can not reflect all the physics of a real flow, the numerical solutions of Laplace's equation

have been validated and used for decades as a primary tool for estimation of aerodynamic load [7] [8].

2.3 Structural domain

As the aerodynamic load act on the surface of an aircraft, the aircraft structure will deform. For this thesis, there is a need for a general method, which can predict a deformation of an arbitrary structure with arbitrary loads. Such a method emerged in aerospace companies in cca. 1950's. After several decades, it evolved to what is known as a Finite Element method (FEM). Although the FEM is used for solving wide variety of problems such as fluid flow, heat conduction or magnetic field, it was originally developed for a structural analysis of swept wings. Therefore in this text the term FEM always refers to a solving of structural mechanics problems.

The virtual work principle The principle of virtual work states that "The virtual work done by the body forces and surface tractions on the virtual displacement, is equal to the work done by stresses on the virtual strains"

$$\delta U = \delta W \tag{2.7}$$

In Equation (2.7) and in Equation (2.8):
U represents the work done by stresses
W represents the work done by body forces

The principle of stationary energy states that "Of all continuous displacement satisfying the geometrical boundary conditions, those that satisfy the equilibrium conduction make the potential energy stationary." For stable structures the potential energy Π in this stationary condition is always minimum,

$$\delta\Pi = \delta U - \delta W = 0 \tag{2.8}$$

in order to satisfy Equation (2.8), the structure is discretized into large number of geometrically simpler sub-structures, called elements. Elements usually share their vertices with other elements. These vertices are called nodes. Using this discretization, the Equation (2.8) is for a steady case expressed as Equation (2.9) :

$$\mathbf{K} \cdot \mathbf{u} = \mathbf{F} \tag{2.9}$$

Where: $\mathbf{K}$ is stiffness matrix of the structure $\mathbf{u}$ is vector of nodal displacements $\mathbf{F}$ is vector of applied nodal loads (forces and moments)

A more detailed explanation of the FEM can be found in literature, a minimal explanation is presented in Chapter 4, where a dealing with large deformations of beam elements is discussed.

2.4 Flight dynamics

2.4.1 Coordinate systems

Three different right-handed coordinate systems are used to solve the equations of motion. The coordinate systems are designated as:

- E - Earth fixed, inertial
- Bf - body fixed, non-inertial
- S - body fixed, non-inertial

The coordinate systems are shown on Figure 2.1, however approach used is this thesis is different than used in literature [9], therefore the systems are briefly explained.

Earth fixed - E is the only inertial reference frame. A Flat Earth approximation is used - the origin is located at surface of the Earth. The Z-axis points outside the earth, X-axis and Y-axis point in arbitrary directions. This is different to the traditional convention of **NED** (North East Down) reference frame [9].

Body fixed - Bf is used for solving of the Equations of motion - Equation (2.10) and Equation (2.11). Its origin is always located at instant center of mass. Initially the axes are aligned with Earth fixed reference frame **E**. As the solution progresses in time, the Body fixed reference frame moves (and rotates) with the aircraft.

Body fixed Structural - S is used to define the geometry and position of **Bf** coordinate system. It's origin is defined by a geometry master model. A convention used here is: The X-axis points to tail, Y-axis points to the right wing, and Z-axis points upwards. As the structure deforms, origin of this axis system remains the same location. While a new position of **Bf** coordinate system is computed, it is always referenced to origin of **S**.

2.4.2 Equations of motion

The equations of motion are solved in non-inertial reference frame **Bf**. The Newton's second law can not be applied directly. A derivation of extensions of the right-hand side can be found in literature [9]. Then the Newton's

second law in non-inertial reference frame is described by Equation (2.10) and Equation (2.11):

$$\dot{\mathbf{v}}^{\mathbf{bf}} = \frac{\mathbf{F}^{\mathbf{bf}}}{m} - \tilde{\omega}^{\mathbf{bf}}\mathbf{v}^{\mathbf{bf}} \tag{2.10}$$

$$\dot{\omega}^{\mathbf{bf}} = \left(\mathbf{J}^{\mathbf{bf}}\right)^{-1}\left[\mathbf{M} - \tilde{\omega}^{\mathbf{bf}}\mathbf{J}^{\mathbf{bf}}\omega^{\mathbf{bf}}\right] \tag{2.11}$$

Note that the force vector $\mathbf{F}^{\mathbf{bf}}$ in Equation (2.10) includes also the gravity force transformed into Body fixed reference frame.

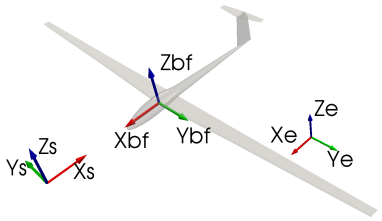

Figure 2.1: Flight mechanics - coordinate systems

Chapter 3

Flow domain solution methods

A fluid motion is traditionally described by set of equations called Navier-Stokes equations [1]. The number of exact solution of Navier-Stokes equations is small. For practical problems, these equations are solved numerically [10].

3.1 Potential Flow

Traditionally Potential flow models are used to determine the aerodynamic load acting on a wing of an airplane. Prandtl's Lifting line theory or Vortex lattice method are most commonly used methods. In this thesis a first order panel method [1] is used. When compared to traditional methods, the way how the load is determined is different.

3.1.1 First order panel method

An approach from VSAERO [4] is used to solve the Laplace's equation - eq. (2.4). Assume a cross section of a wing as shown on fig. 3.1. The surface S_∞ encloses the problem at infinity, surface S represents a body (wing) and surface W represents its wake. The surface $S+W$ divides the domain into two regions: the external region with flow field of interest and velocity potential Φ and the internal region with fictitious flow and velocity potential Φ_i. The surfaces are modeled by a doublet and source singularities.

Green's theorem is applied to both outer and inner region and velocity potential Φ_P is obtained by combining both expressions. [4] The velocity potential Φ_P gives a velocity potential anywhere in the two regions. It is expressed in terms of surface integrals in terms of velocity potential and its normal derivative over the boundary surface as:

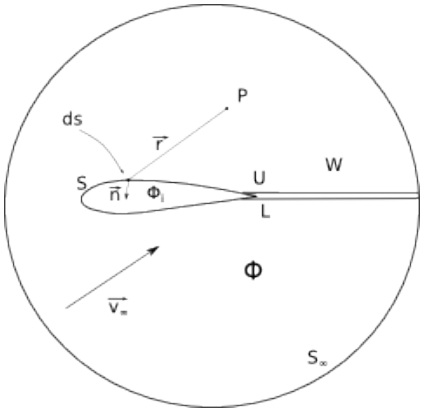

Figure 3.1: Potential flow domain

$$\begin{aligned}\Phi_P = \frac{1}{4\pi}\iint_{S+W+S_\infty}(\Phi-\Phi_i)\,\overrightarrow{n}\cdot\nabla\frac{1}{r}\,dS \\ -\frac{1}{4\pi}\iint_{S+W+S_\infty}\frac{1}{r}\overrightarrow{n}\cdot(\nabla\Phi-\nabla\Phi_i)\,dS\end{aligned} \tag{3.1}$$

Where r is the distance from the point P to the element dS on the surface, and $\overrightarrow{n}$ is unit normal vector of the element dS. [4] The first integral in eq. (3.1) represents disturbance potential from a surface distribution of doublets with density $(\Phi-\Phi_\infty)$. The second integral represents contribution of sources with density $-\overrightarrow{n}\cdot(\nabla\Phi-\nabla\Phi_i)$.[4]

Next, internal Dirichlet boundary condition is introduced. This boundary conditions sets the Internal flow equal to the Onset flow by:

$$\Phi_i = \Phi_\infty \tag{3.2}$$

$$\Phi_P = \Phi_\infty \tag{3.3}$$

In the panel method, the surface is discretized into n surface panels and n_w panels in the wake region,as shown on Figure 3.2 with a constant distribution of singularities, which indicates the first order. When a linear or quadric distribution of panel's sigularities is used, then the method is called second or higher order [1]. The Equation (3.1) is also discretized and the Dirichlet boundary condition is evaluated at centroid of each surface panel. These points are called collocation or control points. Result of this procedure is a linear equation [1] :

$$\sum_{k=1}^{n} C_k \mu_k + \sum_{l=1}^{n_w} C_l \mu_l + \sum_{k=1}^{n} B_k \sigma_k = 0 \tag{3.4}$$

Where C_k, C_l are doublet influence coefficients of body and wake panels, B_k is source influence coefficient, μ_k is doublet strength of body panel, μ_l is doublet strength of wake panel, σ_k is source strength of body panel. The σ_k is set as:

The Equation (3.4) is also used in well recoginzed and validated codes such as VSAERO [4] and PMARC [11]. The main advantage of the panels with constant strength sigularities is that lower quality surface meshes can be used, where the higher order methods require precise meshes without any irregularities [1].

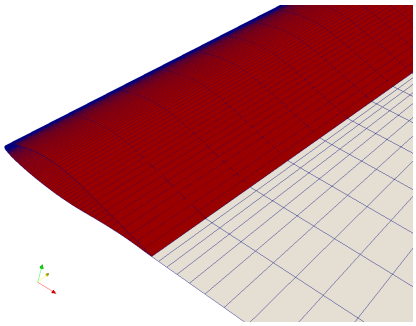

Figure 3.2: Panel method - body panels (red) and wake panels (grey)

$$\sigma_k = \overrightarrow{n_k} \cdot \overrightarrow{Q_\infty} \tag{3.5}$$

Where $\overrightarrow{n_k}$ is the panel normal unit vector and $\overrightarrow{Q_\infty}$ is the freestream velocity.

Chapter 4

Structural domain solution methods

4.1 Finite element method

A Lagrangian formulation of Finite element method for structural analysis was implemented. This method solves the Equation (2.9) as:

$$\mathbf{u} = \mathbf{K}^{-1} \cdot \mathbf{F} \tag{4.1}$$

Where $\mathbf{u}$ is an unknown vector of nodal displacements, later used to compute element nodal forces, $\mathbf{K}$ is stiffness matrix of the whole structure assembled from element stiffness matrices. The assembly process is well described in textbooks. $\mathbf{F}$ is known vector of external load applied at nodes

4.1.1 Beam element

The only element implemented for structural analysis is a two node beam element. It is assumed that a beam element gives an accurate model of a section of a high aspect ratio wing - assuming one element per section. The definition of the beam element is shown on Figure 4.1.

Co-rotational framework The co-rotational framework is a useful tool for computation of element internal elastic forces. It tracks nodal position and rotation. Note that the nodal coordinate system is not aligned with the element coordinate system, as shown on Figure 4.1.

Stiffness matrix of a two node beam element used here is a standard formulation found in textbooks [12] [3].

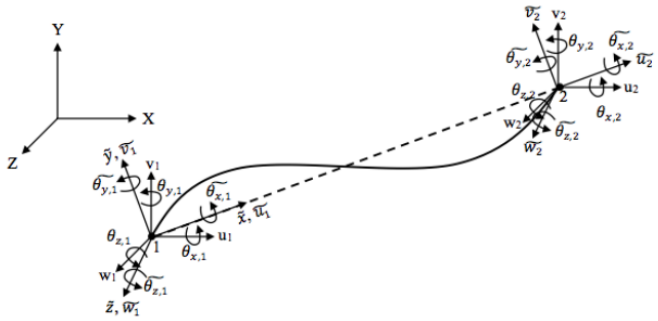

Figure 4.1: Beam element [3]

4.2 Geometrical non linearity in FEM

As shown in Chapter 1 on Figure 1.1 and Figure 1.2, the structure of the wing may deform significantly. Using the Equation (4.1) would introduce large errors, since it assumes small strains and deformations of the structure. For structures undergoing large deformations with small strains an equilibrium between external forces $\mathbf{P_{ext}}$ and internal elastic forces $\mathbf{F_{int}}(\mathbf{u})$ is to be found, as described by Equation (4.2) [3].

$$\mathbf{P_{ext}} = \mathbf{F_{int}}(\mathbf{u}) \tag{4.2}$$

The equation is linearized by perturbing the external load and corresponding nodal displacements, then the Equation (4.2) becomes:

$$\mathbf{P_{ext}} + \mathbf{dP} = \mathbf{F_{int}}(\mathbf{u_0} + \mathbf{du}) \tag{4.3}$$

Solution of Equation (4.3) is then [3] :

$$\mathbf{dP} = \frac{\partial \mathbf{F_{int}}}{\partial \mathbf{u}}\mathbf{du} = [\mathbf{K_T}(\mathbf{u})]\,\mathbf{du} \tag{4.4}$$

The term $\mathbf{K_T}(\mathbf{u})$ in Equation (4.4) is called Tangent stiffness matrix and is expressed as:

$$\mathbf{K_T}(\mathbf{u}) = \frac{\partial \mathbf{F_{int}}}{\partial \mathbf{u}} = \begin{bmatrix} \frac{\partial F_{int,1}}{\partial u_1} & \frac{\partial F_{int,1}}{\partial u_2} & \cdots & \frac{\partial F_{int,1}}{\partial u_m} \\ \frac{\partial F_{int,2}}{\partial u_1} & \frac{\partial F_{int,2}}{\partial u_2} & \cdots & \frac{\partial F_{int,2}}{\partial u_m} \\ \vdots & \vdots & \ddots & \vdots \\ \frac{\partial F_{int,m}}{\partial u_1} & \frac{\partial F_{int,m}}{\partial u_2} & \cdots & \frac{\partial F_{int,m}}{\partial u_m} \end{bmatrix} \tag{4.5}$$

Note that while the stiffness matrix inEquation (4.1) is assembled for unconstrained degrees of freedom, the Tangent stiffness matrix in Equation (4.5) is assembled for all degrees of freedom in the structure.

4.2.1 Newton-Rhapson method

The Newton-Rhapson method is an incremental-iterative technique used to solve set of nonlinear equations, here the Equation (4.4). The solution process is illustrated on Figure 4.2. For the first iteration we compute the first displacement increment $\delta\mathbf{u_1^1}$:

$$\delta\mathbf{u_1^1} = [\mathbf{K_T}(\mathbf{u_0})]^{-1}\,\Delta P = [\mathbf{K_T}(\mathbf{u_0})]^{-1}\,\mathbf{P_{ext,1}} \tag{4.6}$$

Then the residual $\mathbf{R_1^1}$ is computed. The residual is difference between the applied load and internal elastic forces.

$$\mathbf{R_1^1} = \mathbf{P_{ext,1}} - \mathbf{F_{int}}(\mathbf{u} + \delta\mathbf{u_1^1}) \tag{4.7}$$

Then a new displacement increment is computed:

$$\delta\mathbf{u_1^2} = \left[\mathbf{K_T}(\mathbf{u_0} + \delta\mathbf{u_1^1})\right]^{-1}\mathbf{R_1^1} \tag{4.8}$$

This process is repeated until the residual is close to zero. Then the load is incremented and whole process is repeated until the applied load is equal to the prescribed value.

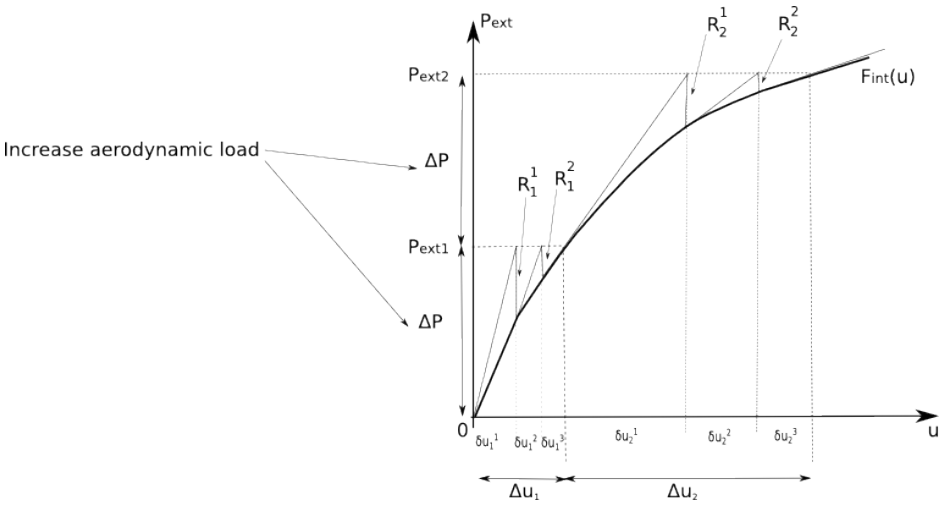

Figure 4.2: Newton-Rhapson method [3]

4.2.2 Numerically generated tangent stiffness matrix

The hardest and most crucial part on geometrical non linearity is a forming of tangent stiffness matrix. It can be done analytically with much labor. Other approach used here is to compute the derivatives from Equation (4.5) Numerically using complex step derivative method. This eliminates the analytical labor and increases accuracy, but also leads to longer computational times.

Chapter 5

Flight dynamics solution methods

A solution of aircraft's equations of motion is straightforward. In this thesis, the forward Euler method is used to numerically integrate the Equation (2.10) and Equation (2.11). The integration process is described by Equation (5.1) and Equation (5.2)

$$\mathbf{v}^{\mathbf{bf}}_{\mathbf{t+\Delta t}} = \int_{t}^{t+\delta t} \dot{\mathbf{v}}^{\mathbf{bf}}_{\mathbf{t}} dt \doteq \dot{\mathbf{v}}^{\mathbf{bf}}_{\mathbf{t}} \cdot \Delta t \tag{5.1}$$

$$\omega^{\mathbf{bf}}_{\mathbf{t+\Delta t}} = \int_{t}^{t+\delta t} \dot{\omega}^{\mathbf{bf}}_{\mathbf{t}} dt \doteq \dot{\omega}^{\mathbf{bf}}_{\mathbf{t}} \cdot \Delta t \tag{5.2}$$

As the new state vector $\mathbf{v}^{\mathbf{bf}}_{\mathbf{t+\Delta t}}\omega^{\mathbf{bf}}_{\mathbf{t+\Delta t}}$ is known, the new position of the aircraft in Earth fixed reference frame is computed.

The time step Δt has to be selected small enough, to avoid unphysical results. Higher order integration schemes, such as Runge-Kutta method were not used due implementation difficulties, however a benefits might be gained from use of adaptive time step. The recent implementation uses only fixed size time step.

Chapter 6

Interaction between domains

6.1 Assumptions

6.1.1 Beam model of a wing

The first and most important assumption is that the wing is of a high aspect ratio and it can be modeled by using one beam (two node) element per section of the wing. Then the finite element model of the wing is assembled as shown on Figure 6.1 The internal elastic forces are evaluated at nodes with respect to element local coordinate system.

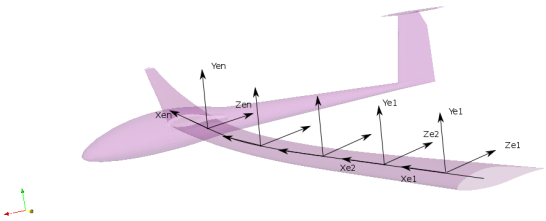

Figure 6.1: Finite element model of a wing and element coordinate systems

6.2 Interacting element

The interaction between flow and structural domain is explained on fig. 6.2. Here a section of a wing is shown. The section consists of n aerodynamic panels, with only one element in span-wise direction. A beam element shares reference nodes of each tip cross section.

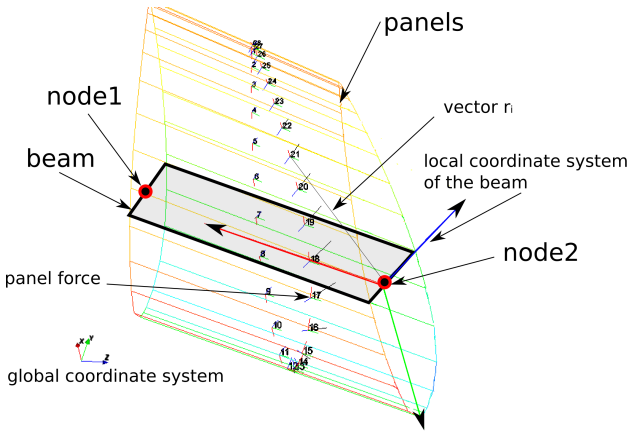

Figure 6.2: Panel method - FEM interaction

6.2.1 Load

The load is applied at the FEM nodes using Equation (6.1) and Equation (6.2). The meaning and application region of f_i and r_i depends on what kind of forces is applied. Both aerodynamic and inertia forces can be applied simultaneously.

$$\overrightarrow{f} = \sum_{i=1}^{n} \overrightarrow{f_i} \tag{6.1}$$

$$\overrightarrow{m} = \sum_{i=1}^{n} \overrightarrow{f_i} \times r_i \tag{6.2}$$

6.2.2 Deformation of the aerodynamic model

The result of the FEM analysis is displacement vector u at each node. Coordinates of aerodynamic panels are updated at each load step using nodal translational and rotational displacements, according to eq. (6.3). Also the nodal coordinates are updated as explained in [3].

$$PTS_{new} = (R_x(\Delta\phi_x)R_y(\Delta\phi_y)R_z(\Delta\phi_z))PTS_{old} + \Delta U \tag{6.3}$$

Where: $\Delta\phi_x, \Delta\phi_y, \Delta\phi_z$, are rotational increments in global coordinate system calculated from last step of Newton-Rhapson iteration, see bellow.

ΔU is displacement increment and $R_x(\phi_x), R_y(\phi_y), R_z(\phi_z)$ are rotational matrices which represent rotation around axes X, Y, Z.

6.3 Unsteady interaction mode

The Newton-Rhapson method is used to compute the deformed shape of the aircraft. The meaning of ”increase load” from Figure 4.2 is however to advance to the next time step, respectively to next flight conditions computed from Equation (5.1) and Equation (5.2). The whole process is illustrated on Figure 6.3.

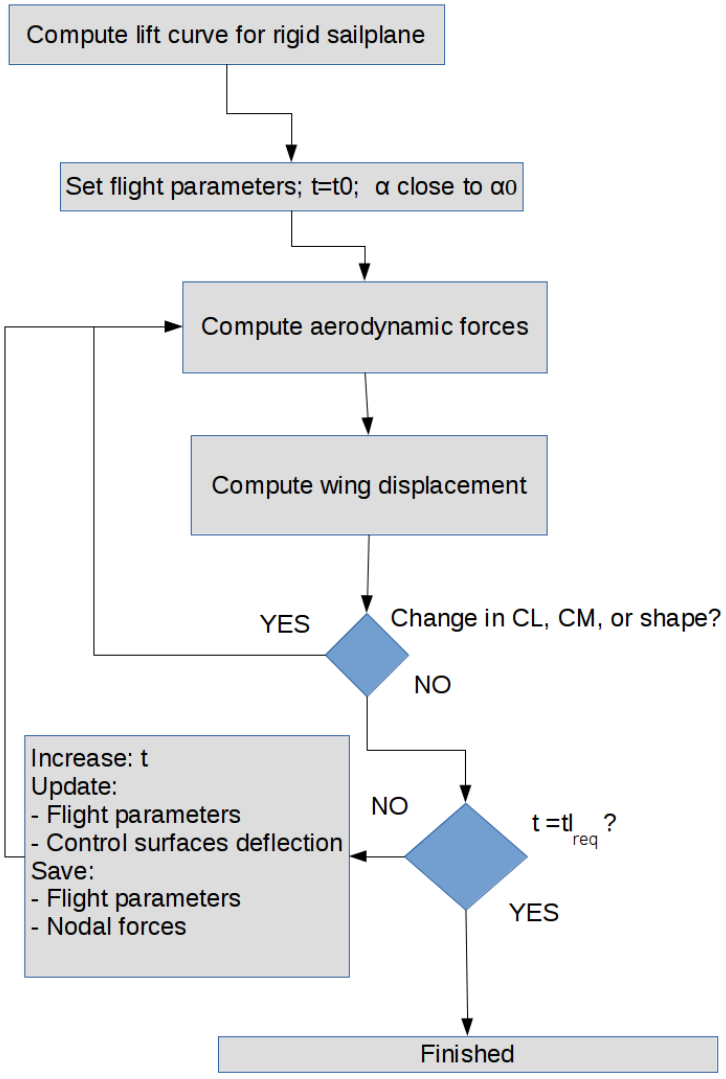

Figure 6.3: Workflow diagram - unsteady mode

Chapter 7

Elastic sailplane - Standard Cirrus 21m

7.1 Introduction and technical data

A fictional sailplane called "Standard Cirrus 21m" has been designed due absence of other geometry and flight test data. The sailplane is a modification of a Standard Cirrus sailplane with wingspan extended to 21m, elongated fuselage and larger horizontal tail. A comparison of the geometry of this fictional sailplane to the original one is shown on Figure 7.1, where the green represents the 21m and red is the original Standard Cirrus.

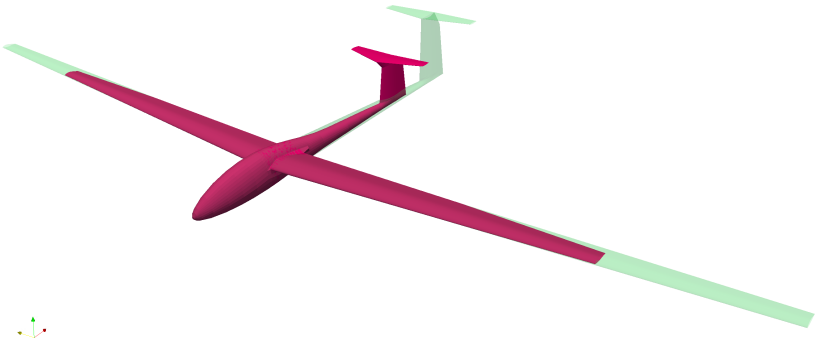

Figure 7.1: Standard Cirrus 21 sailplane - geometry comparison

The technical data of the "Standard Cirrus 21m" is shown in Table 7.1.

Finite element model The wing is divided into 52 span-wise sections. All DOFs are constrained at nodes located at wing-fuselage junction.

Wing span	$21m$
Wing area	$12.4m^2$
Root airfoil	FX S02-196
Tip airfoil	FX-66-17AII-182
Mean chord	$0.696m$
Dihedral	$3°$
Length	$7.9m$
Height	$1.82m$
Aspect ratio	35.5
Weight	$600kg$
CG position	$250mm$ aft ref. pt.*
$\frac{L}{D}_{max}$	43
Maneuvering Speed VA	$180kmh^{-1}$
Never Exceed Speed VD	$240kmh^{-1}$

Table 7.1: Standard Cirrus 21m general characteristics

Wing stiffness and material properties The stiffness an material properties shown in Table 7.2 are assumed to be the same as used in author's initial study [13]. The Young's modulus E and shear modulus G are assumed as constant for whole wing with following values:

$$E = 60GPa$$

$$G = 7GPa$$

The wing has only one spar at $0.25c$ and the nodes are coincident with the spar. Therefore the offset of the elastic axis is almost negligible and both values are assumed to be zero. The span-wise variation of Second moments of area and torsional constant is shown on Figure 7.2. All cross sectional characteristics are given in element local reference frame, as shown on Figure 6.1

7.2 Standard Cirrus 21m maneuver at VA

A response to an abrupt elevator input was analyzed using the unsteady analysis framework described in Section 6.3. As the sailplane features an all-flying tail, the terminology of it's deflection has to be clarified: Negative deflection is denoted as Up direction. It means that the trailing edge travels upwards, the corresponding pilot's input is to pull the stick.

	Symbol	Unit
Cross section area	A_S	m^2
Second moment of area	Iz	m^4
Second moment of area	Iy	m^4
Torsional constant	Jx	m^4
Offset of neutral axis	ΔY_n	m
Offset of neutral axis	ΔZ_n	m
Offset of elastic axis	ΔY_t	m
Offset of elastic axis	ΔZ_t	m
Young modulus	E	N/m^2
Shear modulus	G	N/m^2

Table 7.2: Wing cross sectional properties [13]

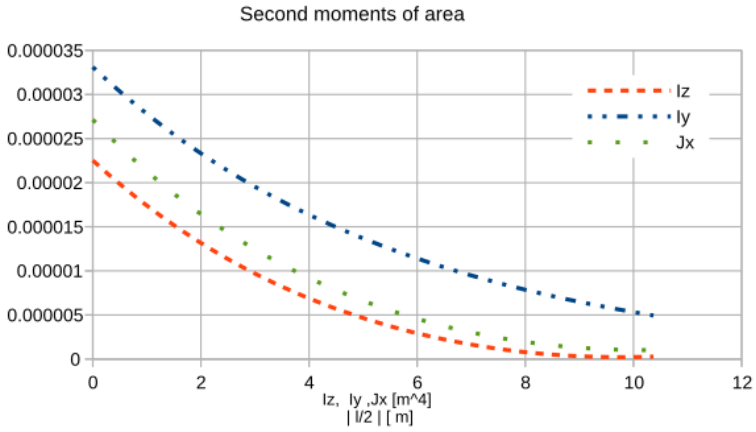

Figure 7.2: Span-wise variation of Iz, Ix, Jy [13]

The elevator input is shown on Figure 7.3a. It consists of a $0.25s$ ramp from $+2°$) position to full up position, $0.75s$ hold. Then $0.5s$ ramp to full down position, and $2s$ hold followed by $0.25s$ ramp to $+2°$ position in order to resume a standard glide path. The time step was set constant $\delta t = 0.02s$.

The maximum load factor is encountered after approx. $0.75s$ for both rigid and elastic case, with maximum value is $n_z = 4.95$, as shown on Figure 7.3c.

7.2.1 Load comparison

The load for rigid and elastic maneuver is compared by using the method of extraction beam element elastic force described in Chapter 4 [3]. The quan-

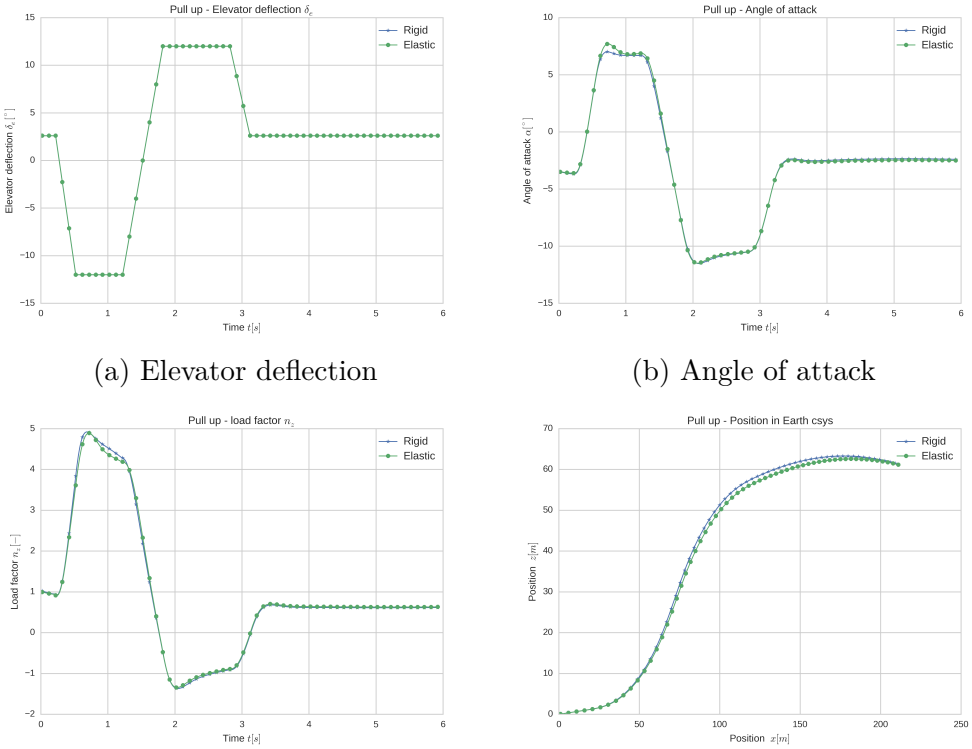

(a) Elevator deflection

(b) Angle of attack

(c) Load factor

(d) Flight path

Figure 7.3: Standard Cirrus 21m sailplane - comparison of rigid and elastic maneuver

tity used for comparison is value of total moment $|M| = \sqrt{{M_x}^2 + {M_y}^2 + {M_z}^2}$ and its individual components. As shown on Figure 7.4, the total bending moment is not changed much by the elastic effects. However a redistribution of its components redistributed significantly.

7.3 Standard Cirrus 21m gust encounter at VA

A gust encounter was analyzed using the same method as maneuver above. The elevator was set at $-2°$ to maintain a logitudinal trim. The time step was set constant $\delta t = 0.01s$. The gust is encountered after a distance of $40m$ is flown. The shape of the gust was taken from [14] as :

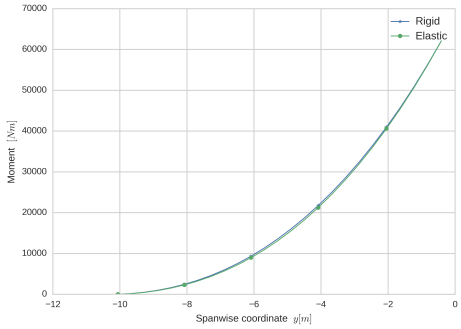

(a) Total moment M

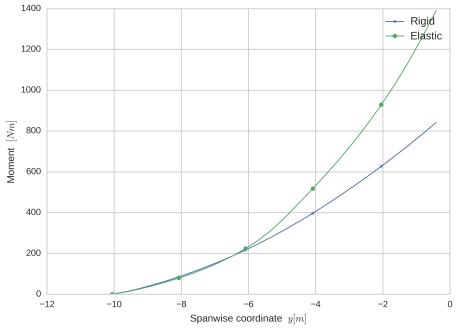

(b) Torsional moment Mx

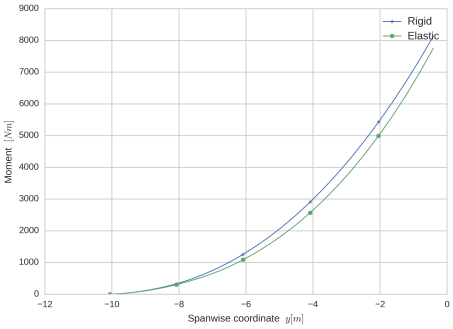

(c) Tangent bending moment MY

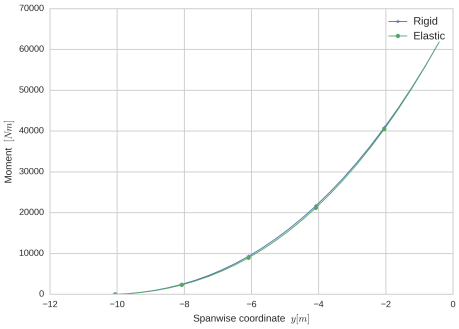

(d) Normal bending moment MZ

Figure 7.4: Standard Cirrus 21m sailplane - comparison of rigid and elastic maneuver - loads

$$W_G(x) = \frac{1}{2} U_{DE} \left(1 - \cos\left(\frac{2\pi x}{25 chord}\right)\right) \tag{7.1}$$

Where U_{DE} is derived gust velocity, assumed to be $U_{DE} = 15.2 ms^{-1}$, x is horizontal distance flown. Only one half-sine wave is assumed.

The load factor increased from $n = 4.35$ to $n = 4.5$

7.3.1 Load comparison

The load for rigid and elastic maneuver is compared by using the same method used to compare loads due maneuver. A sigificant increase in in bending moments can be observed on Figure 7.6.

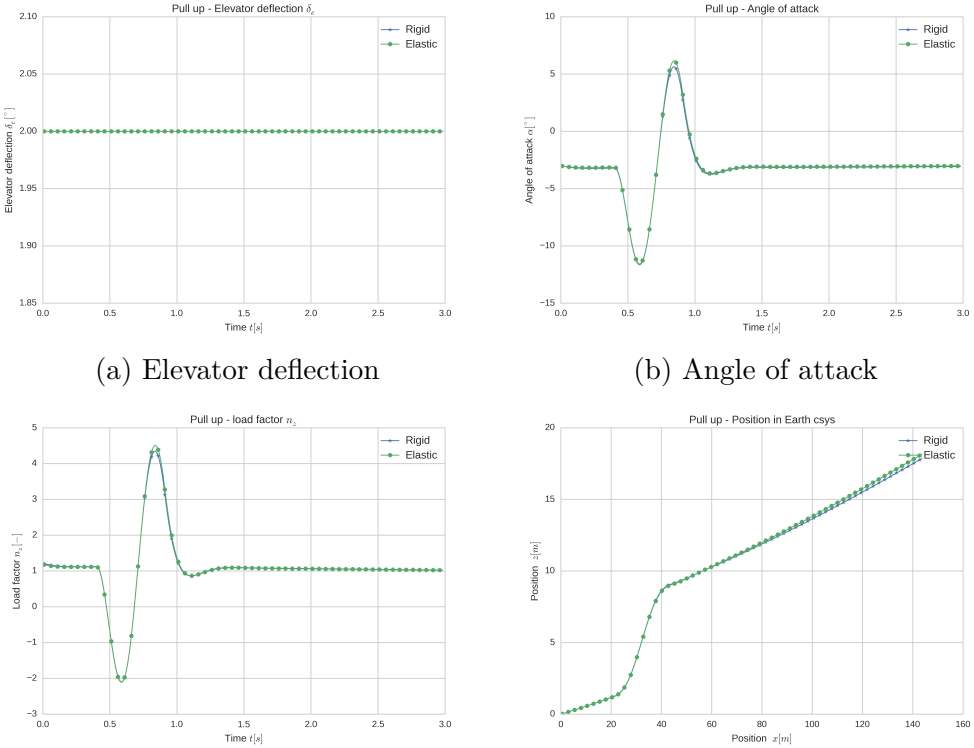

(a) Elevator deflection

(b) Angle of attack

(c) Load factor

(d) Flight path

Figure 7.5: Standard Cirrus 21m sailplane - comparison of rigid and elastic gust response

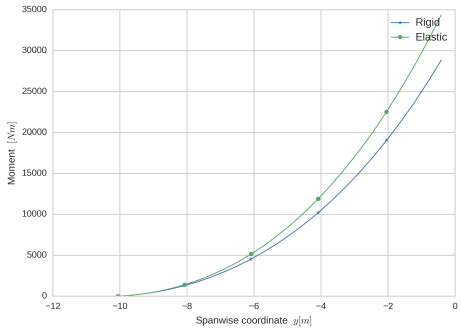

(a) Total moment M

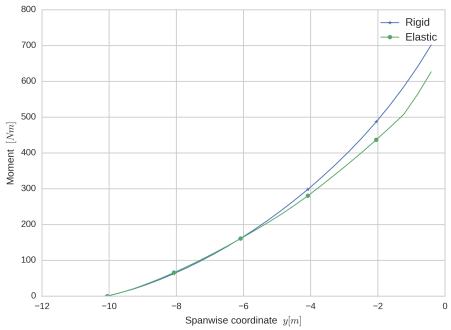

(b) Torsional moment Mx

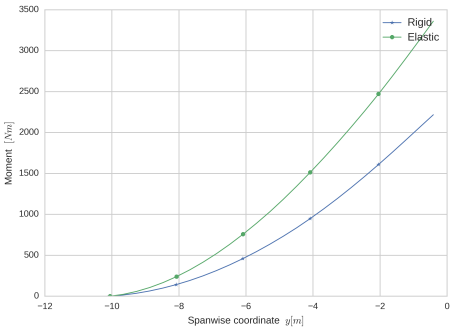

(c) Tangent bending moment MY

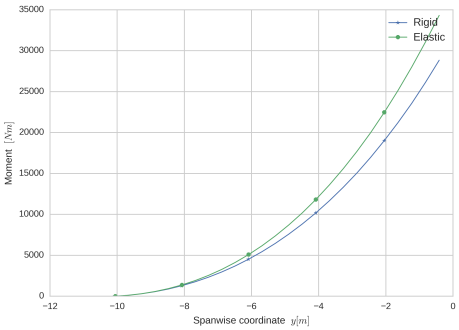

(d) Normal bending moment MZ

Figure 7.6: Standard Cirrus 21m sailplane - comparison of rigid and elastic maneuver - loads

Chapter 8

Conclusion

8.1 Eligibility of the method

A robust method for evaluation of air load of elastic aircrafts has been developed. Compared to other methods, it has relatively low hardware demands, therefore is suitable for use in design organizations which do not have a high performance computer clusters.

8.2 An elastic sailplane

8.2.1 Summary

As the elasticity of a wing changes its aerodynamic characteristics, the traditional approach to load evaluation may be inappropriate. This was demonstrated in Section 7.1.

Maneuver - For a maneuver, there was no significant change in integral flight parameters was observed, comparing rigid and elastic models. A redistribution of load of the elastic wing was observed, as the tangential bending moment increased.

Gust - An increase of load factor was observed, from 4.35 for rigid wing to 4.5 for elastic wing. Also an increase of total load was observed.

8.3 Future work

8.3.1 Improvements of the method

The scope of this thesis was develop a general method for load evaluation of elastic aircrafts, which can be used on average work station. As the method support a modeling of boundary layer effects, the boundary layer was not used when load cases were evaluated. This was mostly due a only quasi 3D implementation of the boundary layer model and due its small impact to overall loads. Next step would therefore be an implementation of more robust and faster (time dependent) boundary layer model. To reduce the computational times and increase accuracy, the parallel programming should be improved. The method can use modern graphical processing units (GPU) [15]. The current implementation used only central processing unit (CPU). Since in 2018 a typical CPU of an average workstation offers 12 to 32 cores and typical GPU offers more than 1024 (less powerful) cores, the speedup may be significant.

8.3.2 Possible use cases

Also an actual comparison of the predicted load and flight characteristic to the actual flight test data is necessary. After a rigorous validation, the method could be used not only to predict loads of elastic aircrafts but also for aeroelastic tailoring. The method is well suited for this task due low hardware demands and relatively fast computational times.

For instance, in Section 7.1, the gust response for the elastic wing was worse than for rigid wing. Eventually, the method could be used to to optimize sailplanes for better responses to gusts.

Bibliography

[1] Joseph Katz and Allen Plotkin. *Low-Speed Aerodynamics*. Cambridge University Press, 2001. ISBN 9780511810329. doi: 10.1017/cbo9780511810329. URL http://dx.doi.org/10.1017/CBO9780511810329.

[2] Antonín Píštěk, O Grégr, V Kahánek, and R Böhm. Pevnost a životnost letadel i. *Vysoké učení technické v Brně, Brno*, 1988.

[3] Sonia Lebofsky. *Numerically Generated Tangent Stiffness Matrices for Geometrically Non-Linear Structures*. PhD thesis, University of Washington, 2013.

[4] B. Maskew. *Program VSAERO Theory Document: A Computer Program for Calculating Nonlinear Aerodynamic Characteristics of Arbitrary Configurations*. NASA contractor report. National Aeronautics and Space Administration, 1987.

[5] EASA. *Certification Specifications for Sailplanes and Powered Sailplanes CS-22*. European Aviation Safety Agency, 2008.

[6] T.E. Noll, J.M. Brown, M.E. Perez-davis, S.D. Ishmael, and G.C. Tiffany. *Investigation of the Helios Prototype Aircraft Mishap - Volume I Mishap Report*. National Aeronautics and Space Administration, 2012. ISBN 9781480279858. URL https://www.nasa.gov/pdf/64317main_helios.pdf.

[7] Vernon J. Rossow. Validation of vortex-lattice method for loads on wings in lift-generated wakes. *Journal of Aircraft*, 32(6):1254–1262, Nov 1995. doi: 10.2514/3.46872. URL http://dx.doi.org/10.2514/3.46872.

[8] NEAL PFEIFFER and TOM ZICKUHR. *Validation of computational aerodynamics applied to general aviationconfigurations*. American Institute of Aeronautics and Astronautics, Jul 1989. doi: 10.2514/6.1989-2169. URL http://dx.doi.org/10.2514/6.1989-2169.

[9] Brian L Stevens, Frank L Lewis, and Eric N Johnson. *Aircraft control and simulation*. Wiley, 2016. ISBN 978-1-118-87099-0.

[10] Alexandre Joel Chorin. Numerical solution of the navier-stokes equations. *Mathematics of computation*, 22(104):745–762, 1968.

[11] D.L. Ashby. *Potential Flow Theory and Operation Guide for the Panel Code PMARC*. National Aeronautics and Space Administration, 1999.

[12] R D. Cook, D S. Malkus, M E. Plesha, and R J. Witt. *Concepts and Applications of Finite Element Analysis: 4th Edition*. 01 2002. ISBN 978-0-471-35605-9.

[13] Pavel Schoř. Aerodynamic load of an aircraft with a highly elastic wing. *Acta Polytechnica*, 57(4):272, Sep 2017. doi: 10.14311/ap.2017.57.0272. URL `http://dx.doi.org/10.14311/AP.2017.57.0272`.

[14] EASA. *Certification Specifications for Normal, Utility, Aerobatic, and Commuter Category Aeroplanes*. European Aviation Safety Agency, 2012.

[15] Nvidia Corporation. *NVIDIA CUDA C Programming Guide*. NVIDIA Corporation, 2701 San Tomas Expressway, Santa Clara, CA 95050, version 3.2 edition, 2010. URL `http://developer.download.nvidia.com/compute/cuda/3_2/toolkit/docs/CUDA_C_Programming_Guide.pdf`.

List of Acronyms

CFD	**C**omputational **F**luid **D**ynamics
DLM	**D**oublet **L**attice **M**method
FEM	**F**inite **E**lements **M**method
VLM	**V**ortex **L**attice **M**method

List of Symbols

c	length	m
dS	infinitesimal surface	m^2
C_D	drag coefficient	-
C_L	lift coefficient	-
C_M	moment coefficient	-
D	drag force	$\mathrm{kg\,m\,s^{-2}}$
L	lift force	$\mathrm{kg\,m\,s^{-2}}$
q	dynamic pressure	$\mathrm{kg\,m^{-1}\,s^{-2}}$
S	area	m^2
$\mathbf{u}$	velocity vector	
$\mathbf{n}$	normal vector	
$\mathbf{f}$	vector of body forces	
$\mathbf{v}$	translational velocity vector	
α	angle of attack	rad
ν	kinematic viscosity	$\mathrm{m^2\,s^{-1}}$
ρ	density	$\mathrm{kg\,m^{-3}}$
ω	rotational velocity vector	